Deep ocean currents detected with satellite altimetry

Jacob L. Høyer[1], Detlef Quadfasel[2] and Ole B. Andersen[1]

1) National Survey and Cadastre (KMS), Denmark

2) Geophysical Department and Danish Center for Earth System Science (DCESS), Niels Bohr Institute,

University of Copenhagen, Denmark

email Jacob Høyer: jlh@kms.dk

Abstract

Overflows of dense and cold bottom water through Denmark Strait and the Faroe Bank Channel are associated with enhanced meso-scale current variability associated with eddies. These fluctuations can be detected through enhanced sea surface height variability in TOPEX/POSEIDON and ERS 1+2 satellite altimeter data. The increased variability coincides with the overflow plumes and has a maximum about 50 km downstream of the Faroe Bank Channel. In Denmark Strait, enhanced variability extends 150 km downstream from the sill with a width of 50-100 km. There is good agreement between variability seen by the different satellites. The satellite observed variability is also in good agreement with in situ observations of temperature and salinity and output from 3-dimensional models of the overflow. Sea surface height data show seasonal variability that may be associated with annual variations of the overflow strength.

1 Introduction

Deep convection that occurs in the Nordic Seas, contributes to the driving of the thermohaline circulation. The deep and dense water flows southward and crosses the Greenland-Scotland ridge, mainly through the two deepest gaps, the Denmark Strait (DS) with a sill depth of 620 meters and the Faroe Bank Channel (FBC) with a sill depth of 840 meters. The transport of bottom water through the straits is on average 1.9 Sv (1 Sv $=10^6$ m^3/s) for the FBC (water colder than 3^oC) and 2.5 Sv for the DS (water colder than 2^oC) (Saunders, 2001). The mean path of the dense bottom waters downstream of the sills is sketched in Figure 1. The cores of the overflow waters (the plumes) generally follow the bathymetry to the right after the sill is crossed but have a small downward component due to bottom friction and entrainment of ambient water. The conditions (density and currents) north of the Scotland-Greenland ridge, upstream of the sills, are fairly stable with only small variations. This is in contrast to observations downstream of the sills where large fluctuations have been observed in temperatures and currents (Dickson and Brown, 1994; Saunders, 1990). The typical periods of the fluctuations are a few days and drifter trajectories and infrared imagery from the DS overflow have related the variability to meso-scale eddies generated where mixing and entrainment is large (Bruce, 1995; Krauss, 1996).

The role of the meso-scale eddies in the FBC was demonstrated in Høyer and Quadfasel (2001) (hereafter HQ2001) where high correlation between current anomalies and temperature fluctuations was found in a mooring array about 140 km downstream of the sill. The existence and generation of meso-scale eddies have also been reproduced in 3-dimensional models of the DS overflow (Jiang and Garwood, 1996; Krauss and Käse, 1998; Jungclaus et al., 2001) suggesting that the DS overflow plume is accelerated by anticyclonic eddies on the shallow side and cyclonic eddies on the deep side of the plume. Until recently, the overflows were thought to be relatively stable on seasonal and longer time scales but new results in Hansen et al. (2001) from the FBC show some seasonal variability and ~25% decrease in the transport over the last 50 years.

The recent high accuracy satellite altimetry missions TOPEX/POSEIDON and ERS 1+2 have revealed many interesting features about the oceanic surface circulation and new results indicate that subsurface processes also can be detected. In HQ2001 it was demonstrated that the overflow variability downstream of the sills can be detected by the T/P satellite as enhanced eddy kinetic energy derived from gradients in the sea surface height (SSH). The maximum in eddy kinetic energy immediately downstream of the sills and the decay further downstream agreed very well with in situ observations from current meter moorings and conductivity-temperature-depth casts. In this paper we will extend the analysis conducted in HQ2001 and show that enhanced variability in SSH is detected in the DS in both the T/P and the ERS data. Estimates of the spatial scales of variability are given for both overflows using the dense spatial sampling of the ERS data whereas the long T/P record is used to examine the seasonal behavior of the variability. Finally, we discuss the importance of errors in the cross-track geoid correction in overflow areas associated with large mean sea surface slopes.

2 In situ observations

The nature of the variability downstream of the overflows is demonstrated in Figure 2, which shows the potential temperature for two repeats of a hydrographic section across the FBC overflow plume. The sections were occupied only 4 days apart on R/V Poseidon cruise 264, August 2000, and are oriented north-south ~30 km downstream of the FBC sill (see Figure 1). The temperature structure varies considerably within these 4 days in particular in the amount of overflow water identified as water below 3^{o}C. The variation is largest in the southern end of the section where the thickness of the plume increases from 70 to 300 meters. The temperature changes in Figure 2 reflect the changes in potential density resulting in a change in steric height of up to 7 cm in the southern part of the section.

The imprint of overflow eddies observed in a FBC mooring array in HQ2001 can also be seen in the Dohrn Bank mooring array in the DS region (Dickson and Brown, 1994). The array is located about 160 km downstream from the sill (Figure 1) and consists of 5 moorings that intersect the mean path of the plume. Figure 3 shows a Hovmüller diagram of the near bottom current and temperature observations for a 10 day window of the 1990 observations. This is typical for the conditions throughout the more than 100 days of observations. The mean is subtracted from every current meter, which has then subsequently been filtered to remove tides. Gray shaded contours show the near-bottom temperatures with a contour interval of 0.5^{o}C and the arrows represent the current anomalies where the velocity scale is given in the lower left. The variability with time-scales of a few days is clearly seen in the temperature observations as four packets of cold water interrupted by three warm events. Temperature variations of more than 2 degrees are associated with current fluctuations of up to 30 cm/s.

The large fluctuations in the overflow plumes in Figures 2 and 3 give rise to changes in SSH. The magnitude of these variations can be estimated from mooring arrays and from shipborne conductivity-temperature-depth (CTD) profiles downstream of the Denmark Strait and Faroe Bank Channel sills. The section 30 km downstream of the FBC (Figure 1) was occupied 5 times within 5.5 days during the Poseidon cruise 264. Figure 2 shows the results from the first two occupations. The steric heights of the 42 profiles were calculated from the bottom up to 50 meters below surface, using the observed temperature and salinity with a vertical resolution of 2 meters. To avoid steric height variability from the mean conditions of the overflow plume, the steric heights are compared from profiles taken within 5 km. The steric height anomalies from these 5 km bins are shown in Figure 4 and it is evident that the fluctuations in the overflow plume are associated with sea surface height variations of several centimeters. The variability in steric height anomalies is largest in the southern part of the section where the variability exceeds 2.5 cm.

Downstream of Denmark Strait, temperature data from the Overflow 73 array (Smith, 1976) and the Dohrn Bank 1990 array were used to estimate the variations in the thickness of the overflow plume. In the core of the overflow, 3 temperature sensors were available in the vertical. The thickness of the overflow plume was determined by interpolation in the vertical between the temperature sensors and the plume was assumed to have the temperature recorded by the near bottom sensor. Linear interpolation was applied but the estimated plume thickness was insensitive to other interpolation methods such as cubic splines. With a plume thickness of 220 meters at the Overflow 73 array and 320 meters at the Dohrn Bank array, the steric height variabilities were 2.1 cm and 1.9 cm, respectively. Knockdown of the mooring can introduce errors in the thickness estimates. Data from a pressure sensor mounted on the shallowest Dorn Bank sensor indicate that the mean knockdown was around 40 meters (which was subtracted the plume thickness) with a standard deviation in the pressure of 31 meters.

About 400 km away from the Denmark Strait sill, 90 CTD profiles were taken during the Variability of Exchanges In the Northern Seas (VEINS) project along the section indicated in Figure 1. The section intersects the overflow plume at a depth of about 1800 meters on the East Greenland slope. Stations along the section were occupied between 6 and 13 times from 1997-2000. The steric heights were calculated over the deepest 500 meters in every profile to exclude seasonal and interannual variability in the upper layers. The mean steric height was removed in every station and the anomalies are shown in Figure 5. It is seen from the figure that the location of the overflow plume coincides with the largest variability in the steric heights anomalies with a maximum variability of 1.7 cm at 33.5^{o}W. This variability is probably related to fluctuations with periods of days because variability with periods longer than ~10 days is small (Saunders, 2001). The results from the various in situ observations are summarized in Table 1. Large steric height variability due to fluctuations in the overflows is found immediately downstream of the sills. The SSH variability in Table 1 is mainly due to changes in the amount of overflow water and not because of changes in the location of the overflow plume. This is indicated in Figures 2 and 3 and corroborated by the additional CTD profiles from the two overflows.

The variability in the overflow plumes agrees well with the pattern of dynamic topography from a dense hydrographic survey downstream of the sill (Krauss and Käse, 1998) where cyclones and anticyclones are associated with changes of several centimeters. In addition, 3 dimensional model results from Jiang and Garwood (1996) suggest that the eddies downstream of the DS are associated with sea surface depressions of up to 7 cm. Jungclaus et al. (2001) find maximum surface depressions of 10 cm. Finally, laboratory experiments have shown that a plume of salty water on a sloping bottom in a rotating fluid was able to generate eddies (Whitehead, 1990).

3 TOPEX/POSEIDON and ERS 1+2 altimetry observations

Sea surface height variations as large as demonstrated above, make it feasible to study the overflows with remote sensing techniques. Infrared imagery has previously been used to detect DS eddies associated with a sea surface temperature (SST) signal (Bruce, 1995) but the method relies on cloud free conditions, which is a rarity in the two overflow regions, and a gradient in SST. There are no significant SST gradients downstream of the FBC and the method can thus not be used to detect eddies here. The radar principle used in the altimetry satellites (Chelton et al., 2001) is independent of cloud cover and SST gradients and measures the height of the surface which is the integral of the processes from the ocean bottom to the surface and not just a measure of skin effects. Density compensated features will not show up as sea surface height changes but the overflows are dense plumes at the bottom and the steric height variability as estimated above will therefore result in equivalent SSH changes. A discrepancy between the satellite observed variability and the steric height estimates may arise from barotropic signals, which are associated with changes in bottom pressure and sea level but not in density and steric heights. The presence of barotropic eddies will thus results in higher SSH variability observed by the satellites compared to the steric height estimates.

3.1 Technical details:

In this study we use TOPEX/POSEIDON (T/P) and ERS 1+2 satellite altimetry observations of SSH that are processed by the Pathfinder team (Koblinsky et al., 1998). The T/P data set is version 8.2 consisting of 294 repeat cycles with a period of 9.92 days (September 1992 to May, 2000). All the standard geophysical, media and instrumental corrections have been applied including the inverse barometer correction and removal of tides with the GOT99.2 tidal model. An edit flag was set by the Pathfinder team if one of the corrections attained unrealistic values. Flagged data were discarded. As shown later, the combination of cross track variations (non-exact repeating ground tracks) and a slope in the mean sea surface may induce a SSH signal that resembles variability from the overflows. In the processing of the data, the Pathfinder team interpolated off track observations to a mean repeat track by using the GSFC00.1 mean sea surface. The correction generally improved the quality of the data, but the uncertainty in the mean sea surface can be significant in regions with large variations in the mean sea surface. With the intention of reducing possible errors from this effect we therefore discarded all observations with a cross track distance of more than 1 km to the exact repeat ground track. Also, observations obtained where the slope in the mean sea surface was greater than 10 cm/km, were removed. This criterion only removed observations on the East Greenland shelf because small mean sea surface slopes (< 4 cm/km in DS and < 2 cm/km in FBC) were found in the regions of the mean paths of the DS and FBC overflow plumes. Outliers were removed (~0.5% of the data) by applying a standard deviation filter with a threshold of 3-σ to the time series at every point. The mean number of T/P observations available in every point is 235 for the Denmark Strait region and 276 for the Faroe Bank region (out of maximum 294). The total percentage of data discarded in the data processing is about 1.5% of the observations, resulting in 232 good repeat cycle observations on the average in the DS region and 272 in the FBC.

The ERS data set is version 5.0 with a total of 81 repeat cycles from the ERS 1 phase C (18 repeat cycles), ERS 1 phase G (13 repeat cycles) and ERS 2 (50 repeat cycles). The repeat period of the ERS satellite is 35 days and observations are available from April 1992 to February 2000 with a gap of ~15 months and an overlap of ~13 months. The Pathfinder team computed the offsets between the different missions and applied the corrections to ensure consistency in the ERS data set. Editing and discarding of bad data was performed in the same way as for the T/P data set described above. However, the 1 km off track criterion was not applied as this reduced the number of observations to 50 % in some tracks in the FBC region. The data processing for DS region discarded 5 observations on the average, reducing the number of observations in each point along the ground tracks from 66 to 61. More observations were available in the FBC region (average of 69 repeat cycles) but the data processing reduced the number of good observations to 60 out of a maximum of 81.

The gridded results shown in the following sections are obtained with an objective gridding routine that uses a second order Markov covariance model of the form

$$C_0(1 + r/a)e^{-r/a}$$

Where C_0 is the data variance, r is the radial distance and a is a correlation scale which was set to 150 km. Additional input to the gridding algorithm is the noise on the data points which will be estimated below.

3.2 Eddy variability

The SSH variability associated with the fluctuations in the two overflows enables the use of satellite altimeter observations to detect the overflows. However, the temporal sampling of the altimetry satellites of 35 (ERS1+2) and 9.92 (T/P) days is too poor to resolve the fluctuations generated by the overflow with periods of a few days. In order to detect the overflows we therefore turn to standard deviations of SSH which is calculated from the timeseries at every point along the ground tracks. The standard deviations were only calculated in points where more than 100 repeat cycles were available for T/P and 30 for the ERS.

The uncertainty in the standard deviations due to the subsampling of 10 and 35 days of the satellites was estimated using a signal with the same spectral characteristics as the observed hourly current observations from the Dohrn Bank array. With a minimum of 30 observations, the standard deviations of the subsampled time series agree within 90% of with true standard deviations, indicating that the reduction in SSH variability due to the 10 and 35 days subsampling of the satellites is small.

The spatial sampling of the T/P satellite in the FBC region is also too low to resolve meso-scale eddies and the results cannot be gridded. The denser sampling with the ERS satellite makes gridding feasible. By using ERS satellite data it is thus possible to give an estimate of the 2-dimensional structure of the enhanced variability from the overflow. The ERS satellite tracks in this region are often displaced from the exact repeat ground track and the 1 km off-track edit criterion would result in less than 30 good observations being present. In order to calculate reliable standard deviation values we therefore did not apply this criterion here but the rest of the data processing was as described in the previous section. As there are no significant gradients in the KMS2000 mean sea surface in this region (< 2 cm/km) inclusion of any off-track data will not introduce serious errors in the results. The minimum number of observations was raised to 40.

Figure 6 shows the gridded SSH variability in the FBC from ERS data where the standard deviations are calculated for every point along the tracks and subsequently gridded. It is evident in the Figure that enhanced SSH variability is observed in several tracks downstream of the sill. The peak of about 9 cm is above the background level of 8 cm and located approximately 50 km downstream of the sill. Enhanced variability is seen in a very localized region with a spatial scale of about 50 km that is similar for directions parallel and perpendicular to the mean path of the overflow. As most of the errors in the altimeter observations have spatial scales larger than 50 km (Tapley et al., 1994) and we only consider enhancements from the background level, we can assume the errors in the SSH variability to be primarily due to the instrument noise of 5 cm for the ERS and 2 cm for the T/P satellites. With the criteria of a minimum of 30 observations for ERS and 100 for T/P, the precisions of the along track standard deviations of SSHs are 0.9 cm for the ERS (0.8 cm for 40 observations) and 0.2 cm for the T/P results. The precisions are used in the objective gridding of the standard deviations and the errors maps suggest a precision of 0.2-0.4 cm for the results shown in Figure 6. The increase of 1 cm in the ERS data is thus significant but more observations are needed to give better and more reliable information about the spatial structure of the variability. Examination of the standard deviation along the central ERS ground tracks reveals that the enhancement in variability exceeds 2 cm for the peak values before gridding.

The results with a 1-2 cm enhancement in SSH variability from the ERS satellite is in good agreement with the in situ observations. The CTD section shown in Figures 2 and 4 is located in the region with enhanced SSH variability in Figure 6 and the estimated steric height variability in Figure 4 is in agreement with the observed enhancement of 1-2 cm. The spatial scales of 50 km of the variability corresponds to the width of the overflow plume as seen in Figure 2 and to the size of the meso scales eddies which have been seen in models results (Krauss and Käse, 1998; Jungclaus et al., 2001; Shi et al., 2001).

The latitude of the DS is close to the turning latitude (66.2 deg.) of the T/P satellite, which gives a much better spatial sampling here. Standard deviations of SSH from both the T/P and ERS can be gridded and the two independent satellite estimates compared. The inter-comparison was not possible for the eddy kinetic energy values in HQ2001 because the higher ERS noise combined with the fewer observations blurred the signal from the overflows. The standard deviation of SSH in Figure 7 shows that both satellites are able to detect enhanced SSH variability downstream of the sill in the DS. Despite the different spatial and temporal sampling of the two satellites the shape of the enhanced variability is similar with a peak in variability on the East Greenland slope, extending about 100-150 km downstream from the sill to the Dohrn Bank array. The errors in the objective gridding are 0.2-0.3 cm for the ERS results and 0.1-0.2 cm for the T/P.

The level of the ERS background variability is higher and less uniform than the T/P data due to higher noise and fewer observations but the enhancement of up to 4-5 cm is the same for the two satellites. The increase in SSH variability immediately downstream of the sill agrees well with Table 1 and the satellite observed enhancements of 2-3 cm at the positions of the Overflow 73 and Dohrn Bank array correspond to the steric height estimates. Both satellites display enhanced variability further downstream along the east Greenland slope to about 64.3^{o}N. SST observations from the AVHRR satellite suggest that the contribution from other processes such as frontal instabilities along the East Greenland Front may be larger in this region than closer to the sill. The SST change across the front is very large (up to 7^{o}C) hence frontal instabilities would be associated with a SST signal. After removal of the annual and semiannual harmonic from 6 years of daily SST data, the maximum variability is associated with the front around 65^{o}N centered at the 500 m depth contour. While these frontal processes are small and most likely unimportant immediately downstream of the sill they can influence the altimeter data further downstream and the 1 cm SSH variability change from 64.3^{o}N to 65^{o}N may arise from overflow eddies, frontal processes or a combination of the two. However, with the results from the VEINS CTD section in Figure 5, it is now clear that the fluctuations in the deep overflow can account for this variation in SSH, hence the contribution from the frontal processes to the SSH variability is probably low. A high-pass filter with a cutoff of 50 days was applied to the T/P data before calculating the variability. Except for a general lowering of the background noise levels there was little change in the detection of the overflow plume indicating that seasonal and processes with longer period do not generate the elevated SSH variability which is seen in Figure 7.

It is thus clear that the deep variability in the overflow plumes is not density compensated and can be detected as enhanced SSH variability by the altimeter satellites. The satellite results from the two overflows are consistent with the in situ data, with a maximum in SSH variability immediately downstream of the sill where in situ observations suggest the largest fluctuations to occur. The spatial scales of the regions with enhanced variability correspond to the size of meso-scale eddies of 20-70 km which have also been seen with drifters and in 3 dimensional models of the DS overflow (Krauss, 1996; Jiang and Garwood, 1996; Jungclaus et al., 2001). In addition, the increase in SSH variability in Figures 6 and 7 corresponds very well to the T/P derived eddy kinetic energy results presented in HQ2001 (their Figure 5) except for the width of the DS overflow that tends to be wider for the SSH standard deviation results.

3.3 Seasonal variability

With the increasing observation period of the satellite missions we can reliably calculate the standard deviation of SSH for the 4 seasons for the two overflows throughout the period of observations. Only results from the T/P satellite will be shown here because seasonal estimates are based upon a quarter of the observations used in the previous sections. Thus, with standard deviations of SSH based upon 10-20 observations (compared to ~60 for all the record) the uncertainty in the ERS results is too high compared to the signal we want to detect. The seasonal behavior of the variability was examined in two T/P ground tracks, located in the regions with enhanced variability through all the years and perpendicular to the mean paths of the overflow (see Figure 6 for FBC and Figure 7 for DS). Bad observations were discarded in the same way as in the previous section, but the criteria of minimum observations was lowered to 25 observations per season. Figure 8 shows the results from the DS and FBC regions, where the variability is calculated for the individual seasons throughout all years of the record and subsequently smoothed along track with a three-point running mean. The peaks in SSH variability are clearly seen during all seasons for both overflows, even though the uncertainty in the estimates are higher due to the reduced number of observations. In the Denmark Strait, the number of available observations decreases towards the East Greenland coast due to ice contamination. However, the standard deviations for the peak values in Figure 8a are all based upon a minimum of 40 observations and the precision is therefore 0.3 cm. The ice free conditions in the Faroe Bank channel region result in better data return and the standard deviations in Figure 8b are based upon minimum 60 observations (precision of 0.26 cm). Error bars are added according to these results.

The background noise level is defined to be the SSH variability in the ground tracks which is found outside the peaks associated with the overflows (e.g. south of 61.5^{o}N in FBC and east of 27^{o}W in the DS). It is seen from Figure 8 that the seasonal differences are primarily due to variations in this background noise level with a maximum during winter (Dec-Jan-Feb) and minimum during summer (June-July-Aug). The other satellite observations away from the overflow plume display a similar seasonal cycle in the variability, which is probably due to variations in the amount of eddies generated by the wind. White and Heywood (1995) related seasonal varying eddy kinetic energy of the subpolar North Atlantic to changes in wind forcing and Stammer and Wunsch (1999) found a significant correlation between eddy kinetic energy and wind forcing in 10 by 10 degree areas in the eastern North Atlantic. In addition, Stammer et al. (2001) used an eddy resolving model of the North Atlantic to show the importance of high-frequency wind forcing in generating eddy kinetic energy.

Figure 8b reveals the differences between the DS and the FBC: The DS increase above the background level is relatively constant for all the seasons with an increase of 4-5 cm but the FBC overflow shows some seasonal variation. The late fall (Sep-Oct-Nov) increase is of 1-2 cm above the background level of ~4 cm. This is significantly lower than the summer (June-July-Aug) values, where the background level of ~3 cm and the peak variability of ~6.5 cm represent an enhancement of up to 3.5 cm due to fluctuations in the overflow plume. It is not yet clear if these variations are related to changes in the transport or the density of the overflow, but sensitivity studies with a high resolution model of the overflows could give insight into this matter.

4 Limitations: Off-track geoid correction in other overflows

Overflow of dense bottom water from one basin to another is an important mechanism for the distribution of water masses throughout the world oceans. Several important overflows such as the Charlie-Gibbs Fracture Zone, the Mediterranean outflow and the Romanche Fracture Zone overflow exhibit fluctuations and mixing similar to the FBC and the DS (Saunders, 1994; Iorga and Lozier, 1999; Polzin et al., 1996). With the above findings it is therefore interesting to extend the analysis to these regions. However, large mean sea surface slopes up to 10 cm/km combined with errors in the cross-track interpolation limit the investigation. The example shown here is from the Mediterranean outflow where dense salty water flows into the Atlantic through the Strait of Gibraltar and experiences strong mixing in the Gulf of Cadiz.

With the same data processing as used above, including the cross track geoid correction and only using observations within a 1 km cross track limit, the variability along the track is shown in Figure 9a. The signal looks promising as it is close to where the ground track crosses the overflow plume and in the region of large mixing. But an analysis of the gradients in the KMS2000 mean sea surface (Figure 9b) reveals that large gradients perpendicular to the ground tracks of up to 8 cm/km coincide with the increase in SSH variability. It is thus not clear whether the enhancement in Figure 9a is due to mixing processes in the Mediterranean outflow plume or arise from an incorrect correction of observations up to 1 km away from the exact repeat ground track. The error in the correction is small in the FBC and DS overflow regions with mean sea surface slope values less than 4 cm/km but overflow regions with large mean sea surface slopes such as the Charlie-Gibbs fracture Zone and the Romanche Fracture zone need special attention for cross track geoid correction. Until the sources of the suspicious increases in variability are determined, satellite altimeter data should be used with caution when small scale studies are performed in regions with large gradients in the mean sea surface.

5 Final Comments

The use of ERS altimetry data with higher spatial sampling than T/P makes it possible to give an estimate of the structure of the enhanced variability downstream of the FBC sill. The overflow variability detected by the satellite is centered about 50 km downstream of the sill and has a scale of 50 km, which is the same for the direction along and perpendicular to the plume. The satellite observed variability is in good agreement with estimates of steric height anomalies from a CTD section about 30 km downstream of the sill.

In DS, the results from the two independent satellite missions are consistent despite differences in spatial and temporal sampling. A maximum in SSH variability is located on the western side of the Denmark Strait, immediately downstream of the sill. The variability level is generally higher in the ERS data due to higher noise but the enhancement of up to 5 cm associated with the overflow is in good agreement with the T/P results as well as the spatial extent of ~150 km from the sill. In situ observations from moorings support the satellite results with a large variability in the overflow plume immediately downstream of the sill. The results with enhanced mixing and entrainment between the sill and the Dorhn Bank array are also supported by the results in Dickson and Brown (1994). They found the largest deceleration and downward velocity of the overflow and ascribed it to enhanced entrainment of ambient water in this region.

Further downstream, in situ results from a VEINS section along 64.3^{o}N suggest that the observed variability increase of ~1 cm on the East Greenland slope is due to variability in the overflow plume. Laboratory experiments, drifter tracks and several 3 dimensional models of the overflows corroborate the satellite observations of enhanced variability downstream of the sills due to large mixing and entrainment and associated meso scale eddies.

It is evident from seasonal statistics that both overflows can be detected by the T/P during all seasons with an annual cycle in the background variability levels probably related to variations in the wind generated eddies. The DS anomaly in SSH variability above the background noise level is relatively constant of 4-5 cm for the different seasons. More seasonal variability is seen in the FBC where the overflow is only weakly detected during fall but very clear in the summer. It is not clear at the moment how these variations relate to the observed seasonal changes in the overflow transport by Hansen et al. (2001). The seasonal changes are from one T/P ground track intersecting the plume and the satellite signal could arise both from a weakening in the mixing and eddy generation or from a shift of the mixing region along the overflow pathway. A longer ERS time series can answer the question as well as sensitivity studies with a high resolution model of the overflows can help to clarify how changes in the transports are reflected as changes in the mixing. With the findings here there is thus a potential that long satellite altimetry time series can be used to monitor changes in the two overflows which make a significant part of the global thermohaline circulation.

Acknowledgements

The work is carried out under the GEOSONAR project funded by the Danish Natural Research Councils Earth observation program. The NASA Ocean Altimeter Pathfinder team is acknowledged for providing the altimetry data and the VEINS project for the CTD data in the DS region. The R/V Poseidon cruise was financed by the University of Hamburg, Germany.

Figure Captions

Sill		**Distance from sill (km)**	**Maximum SSH std. deviation (cm)**
Denmark Strait	Record length (days)		
	32	55	2.1
	120	160	1.9
	Number of CTD profiles		
	90	400	1.7
Faroe Bank Channel	42	30	2.9

Table 1. *Steric height variability due to fluctuations in the DS and FBC overflows, estimated from in situ observations.*

Figure 1. *Bathymetry of the North Atlantic in gray shading. The thin dotted line indicate the mean path of the overflow water through the Denmark Strait and the Faroe Bank Channel. The Dohrn Bank (DB) and Overflow 73 (OVF73) mooring*

arrays are indicated with circles and triangles mark the position of the CTD observations downstream of Denmark Strait sill (from VEINS data) and of the FB sill (from Poseidon 264 data).

Figure 2. *Potential temperature from 2 repeats of the section about 30 km downstream of the Faroe Bank Channel sill, which is indicated with triangles in Figure 1. Contour interval is 1^oC. The lateral positions of the profiles are marked with the small numbers in the top of each plot and the vertical sampling interval of the CTD observations is 2 meters. The time and dates of the observations in 1999 are marked on the Figure.*

Figure 3. *Time-distance plot of near-bottom temperatures (gray shadings) and current anomalies (arrows). The data are from 5 moorings from the Dohrn Bank 1990 mooring array about 160 km downstream of the Denmark Strait (see Figure 1 for positions). The currents have been filtered to remove effects from tides and the scale is indicated by the horizontal arrow in the lower left. The contour interval for the temperatures is 0.5^oC and the distance is calculated from the southernmost mooring.*

Figure 4. *Steric height anomalies (triangles, left axis) calculated from CTD profiles along the section 30 km downstream of the Faroe Bank Channel sill (see Figure 1). The depth in meters is shown in solid (right axis). The anomalies are relative to mean values calculated at the positions marked with dots. All CTD casts are taken within 5.5 days in August 1999.*

Figure 5. *Same as Figure 4, except the CTD section is located about 400 km downstream of the Denmark Strait sill (see Figure 1). The profiles are taken from 1997 to 2000 and the steric heights are calculated over the deepest 500 meters.*

Figure 6. *Gridded standard deviation of ERS 1+2 SSH observations (colors) and bathymetry (contours) in the Faroe Bank Channel region. The positions of the ERS ground tracks are overlaid in black and only observations obtained at depths >300 m have been used. The red dots indicate the T/P ground track used in Figure 8a and the black dashed line indicates the sill.*

Figure 7. *Denmark Strait standard deviation of SSH from the T/P (top) and the ERS 1+2 (bottom) satellites. The bathymetry is contoured and satellite ground tracks are overlaid in black. Only observations over water depths >300 m have been used. The yellow line indicates the ground track used in Figure 8b and the sill is indicated with the bold dashed line.*

Figure 8. *SSH variability calculated from the T/P for the different seasons: December-January-February (DJF), March-April-May (MAM), June-July-August (JJA) and September-October-November (SON). a) Along a ground track ~30 km from the Faroe Bank Channel sill (see positions in Figure 6). b) Results from a ground track in the Denmark Strait (see positions in Figure 7).*

Figure 9. *a) Sea surface height variability downstream of the Mediterranean outflow along the T/P ground track shown with thick white dashed line in b). b) Magnitude of the KMS2000 mean sea surface gradient perpendicular to the white T/P ground track (gray shadings). The thin dashed contour lines denote the bathymetry.*

References

Bruce, J. G. (1995). Eddies southwest of the Denmark Strait, *Deep-Sea Research*, Vol. 42, No. 1, pp.12-29.
Chelton, D. B., Ries, J. C., Haines, B. J., Fu, L.-L. and Callahan, P. S. (2001) Satellite Altimetry, *In: Satellite Altimetry and Earth Sciences, a Handbook of Techniques and Applications, Edited by Fu and Cazenave*, International Geophysics series, Vol. 69, pp. 1-131.

Dickson, R. R. and Brown, J. (1994). The production of North Atlantic Deep Water: Sources, rates and pathways, *Journal of Geophysical Research*, Vol. 99, No. C6, pp. 12319-12341.
Hansen, B. and Østerhus, S. (2000). North Atlantic-Nordic Seas exchanges. *Progress in Oceanography*, Vol. 45, pp. 109-208.
Hansen, B. Turrell, W. R. and Østerhus, S. (2001). Decreasing overflow from the Nordic Seas into the Atlantic Ocean through the Faroe Bank Channel since 1950, *Nature*, Vol. 411, pp. 927-930.
Høyer, J. L. and Quadfasel, D. (2001). Detection of deep overflows with satellite altimetry, Geophys. Res. Letters, Vol. 28, No. 8, pp. 1611-1614.
Iorga, M. C. and Lozier, S. M. (1999). Signatures of the Mediterranean outflow from a North Atlantic climatology 1. Salinity and density fields, *Journal of Geophysical Research*, Vol. 104, No. C11, pp. 25985-26009.
Jiang, L. and Garwood, W. J. (1996). Three-dimensional Simulations of Overflows on Continental Slopes, *Journal of Physical Oceanography*, Vol. 26, pp. 1214-1233.
Jungclaus, J. H., Hauser, J. and Käse, R. H. (2001). Cyclogenesis in the Denmark Strait Overflow Plume, *Journal of Physical Oceanography*, Vol. 31, pp. 3214-3229.
Koblinsky, C. J., Ray, R. D., Beckley, B. D., Wang, Y.-M., Tsaoussi, L., Brenner, A. and Williamson, R. (1998). NASA Ocean Altimeter Pathfinder Project Report 1: Data Processing Handbook, Technical report NASA/TM-1998-208605, Goddard Space Flight Center, National Aeronautics and Space Administration, pp 1-55.
Krauss, W. (1996). A note on overflow eddies, *Deep-Sea Research*, Vol. 43, pp. 1661-1667.
Krauss, W. and Käse, R. H. (1998). Eddy formation in the Denmark Strait overflow, *Journal of Geophysical Research*, Vol. 103, No. C8, pp. 15525-15538.
Polzin, K. L., Speer, K. G., Toole, J. M. and Schmitt, R. W. (1996). Intense mixing of Antarctic Bottom Water in the equatorial Atlantic Ocean, *Nature*, Vol. 380, pp. 54-57.
Saunders, P. M. (1990). Cold Outflow from the Faroe Bank Channel, *Journal of Physical Oceanography*, Vol. 20, pp. 29-43.
Saunders, P. M. (1994). The flux of overflow water through the Charlie-Gibbs Fracture Zone, *Journal of Geophysical Research*, Vol. 99, No. C6, pp. 12343-12355.
Saunders, P. M. (2001). The Dense Northern Overflows, *In Ocean Circulation & Climate, edited by Siedler, Church and Gould*, International Geophysics series, Vol. 77, pp. 401-418.
Shi, X. B., Røed, L. P. and Hackett, B. (2001). Variability of the Denmark Strait Overflow: A numerical study, *Journal of Geophysical Research*, Vol. 106, No. C10, pp. 22277-22294.
Smith, P. C. (1976). Baroclinic instability in the Denmark Strait overflow, *Journal of Physical Oceanography*, Vol. 6, pp. 355-371.
Stammer, D. and Wunsch, C. (1999). Temporal changes in eddy energy of the oceans. *Deep-Sea Research II*, Vol. 46, pp. 77-108.
Stammer, D. and Böning, C. and Dieterich, C. (2001). The role of variable wind forcing in generating eddy energy in the North Atlantic. *Progress in Oceanography*, Vol. 48, pp. 289-311.
Tapley, B. D., Ries, J. C., Davis, W. G., Eanes, R. J., Schutz, B. E., Schum, C. K., Watkins, M. M., Marshall, J. A., Nerem, R. S., Putney, B. H., Klosko, S. M., Luthcke, S. B., Pavlis, D., Williamson, R. G. and Zelensky, N. P. (1994). Precision orbit determination for TOPEX/POSEIDON, *Journal of Geophysical Research*, Vol. 99, pp. 24383-24404.
White, M. A. and Heywood, K. J. (1995). Seasonal and interannual changes in the North Atlantic subpolar gyre from GEOSAT and TOPEX/POSEIDON altimetry. *Journal of Geophysical Research*, Vol. 100, No. C12, pp. 24943-24954.
Whitehead, J. A., Stern, M. E., Flierl, G. R. and Klinger, B. A. (1990). Experimental Observations of Baroclinic Eddies on a Sloping Bottom. *Journal of Geophysical Research*, Vol. 95, No. C6, pp. 9585-9610.

Figure 1:

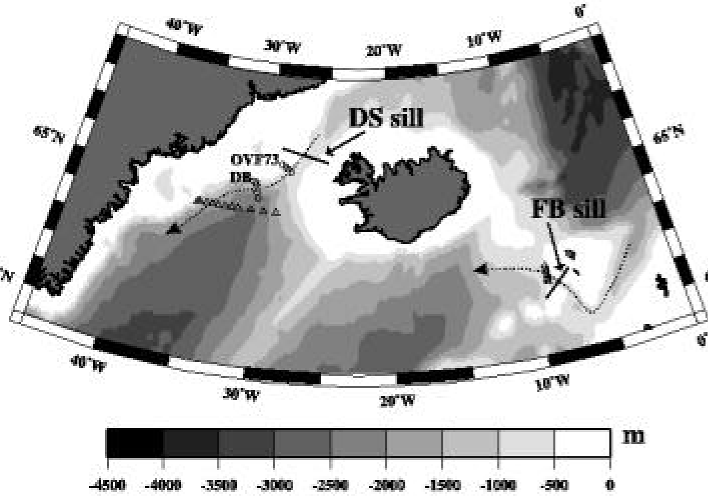
DS sill
FB sill
OVF73
DB
40°W
30°W
20°W
10°W
0°
65°N
60°N
m
-4500
-4000
-3500
-3000
-2500
-2000
-1500
-1000
-500
0

Figure 2:

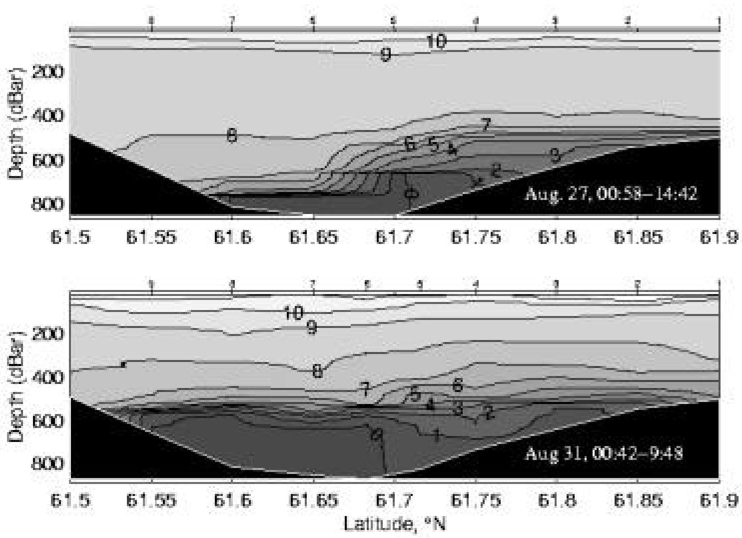
Depth (dBar)
Aug. 27, 00:58–14:42
Aug 31, 00:42–9:48
Latitude, °N
61.5
61.55
61.6
61.65
61.7
61.75
61.8
61.85
61.9

Figure 3:

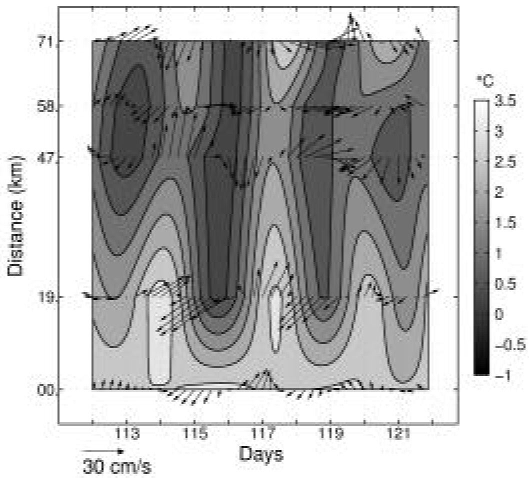

Figure 4:

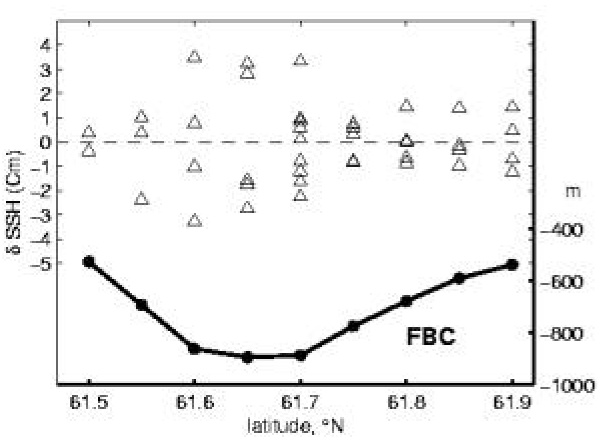

Figure 5:

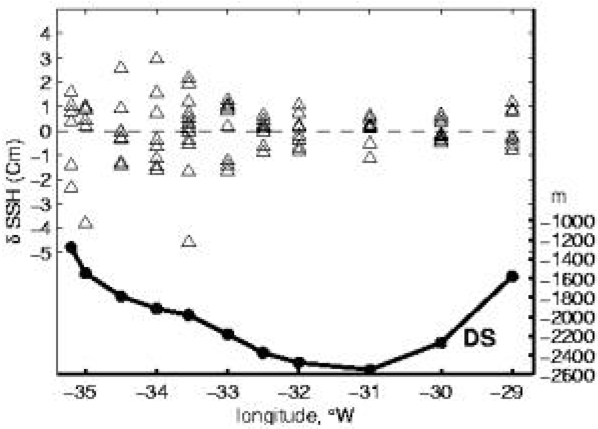

Figure 6:

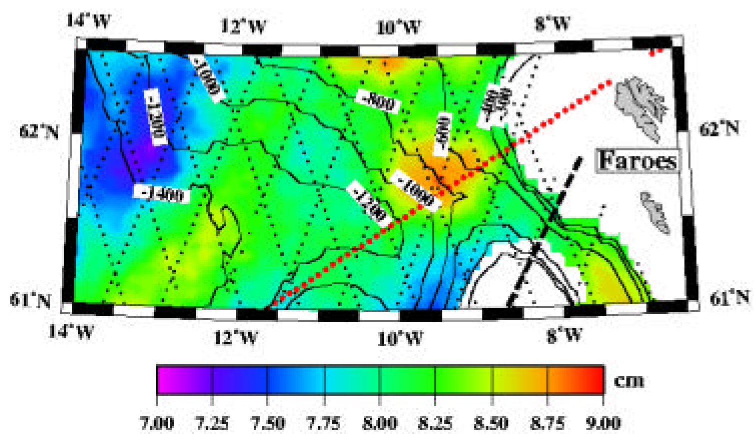

:

Figure 7:

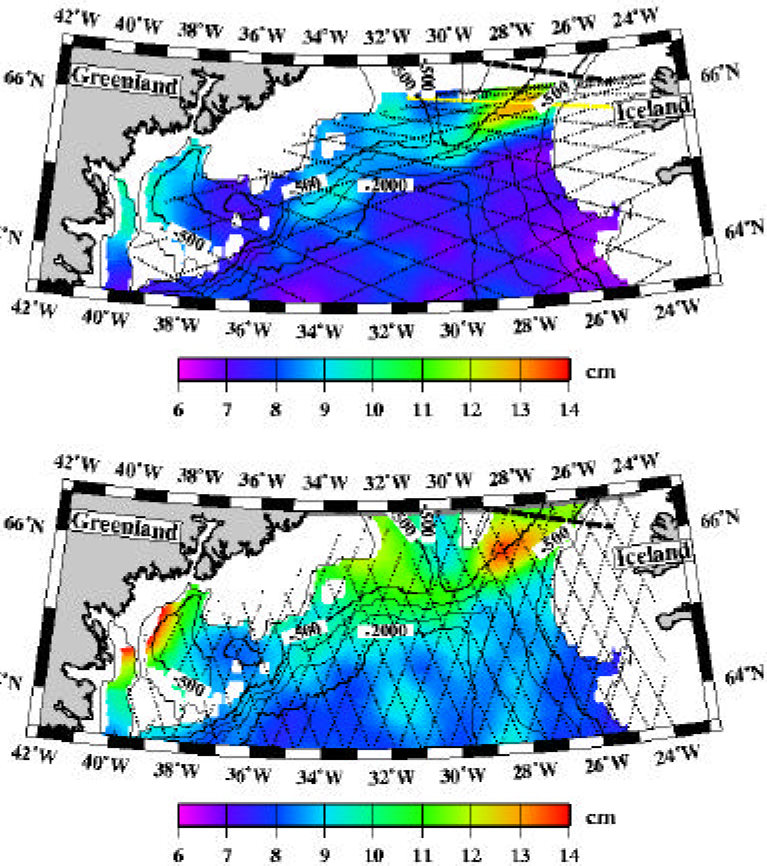

Figure 8:

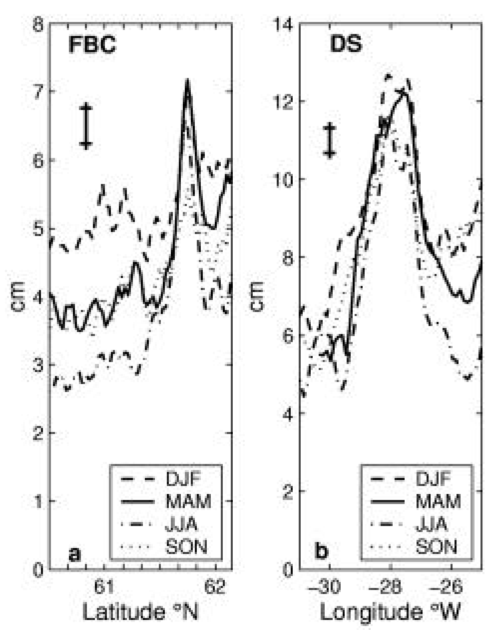

Figure 9: